Growth of Binary Oxide Nanowires

Jiangxiong Wang, Sishen Xie, and Weiya Zhou

Abstract

One-dimensional (1D) semiconducting oxide nanostructures such as ZnO, SnO_2, and In_2O_3 have been extensively studied due to their excellent optical and electrical properties. Growth of 1D nanostructures with precisely controlled size, phase purity, crystallinity, and chemical composition still presents numerous challenges. In this review, we report the recent progress on the synthesis of binary oxide nanostructures consisting of different oxides through a simple and effective vapor transport approach in our research. By controlling the experimental conditions, this approach enables the synthesis of various multicomponent binary oxide nanowires.

Introduction

Semiconducting oxides have been extensively studied in the past ten years due to their outstanding optical and electronic properties. Among them, ZnO, SnO_2, and In_2O_3 are three key wide-bandgap semiconducting oxides. Their one-dimensional (1D) nanostructures have been the subject of significant research efforts in recent years and have been demonstrated to possess better optical and electronic properties than the bulk materials.[1–3] Nanodevices based on these nanostructures, including light-emitting diodes, ultraviolet lasers, optical waveguides, and chemical sensors, have been reported in the past few years.[4]

The fabrication of complicated functional nanostructures is a crucial step toward the realization of functional nanodevices. To meet the requirements of optoelectronics at the nanoscale, researchers are trying to fabricate more complicated nanostructures such as superlattice nanowires,[5] hierarchically assembled structures,[6] and heterostructures along the axial and radial directions of nanowires.[7]

The synthesis of simple oxide nanostructures has progressed greatly in the past few years, and 1D oxide nanostructures with various morphologies, including nanowires,[8–10] nanotubes,[11] and nanobelts,[12] have been successfully produced by different methods. However, the synthesis of functional and composite oxide nanostructures is still suffering from many problems such as low yield, lack of reliability, and complex procedures. One-dimensional binary oxide nanostructures formed of different materials may combine the physical properties of the different materials into one nanostructure. Moreover, due to the joining of two individual materials with different bandgaps into heterostructures, the composite nanostructures are expected to possess some novel electric transport and optical properties. Therefore, the fabrication of composite oxides and investigation of their growth behavior are becoming more and more attractive.

In this review, recent progress in our research on growth of 1D binary oxide nanostructures will be summarized. We focus on developing a simple and effective approach to *in situ* synthesis of binary oxide nanostructures consisting of two different oxides such as ZnO, SnO_2, and In_2O_3. Our strategy to synthesize and design binary oxide nanostructures is based entirely on a bottom-up, vapor-phase transport (VPT) method. It will be shown that this method allows controlled growth of novel binary oxide nanostructures with various morphologies.[8,14,16,18]

Growth of ZnO-SnO_2 Composite Structures

Composite ZnO-SnO_2 nanostructures were grown in a horizontal tube furnace using the modified vapor-phase transport (VPT) method.[13] SnO and ZnO powders were used as the reactant source and were separately loaded in a quartz boat following the stream direction. Silicon substrates with a thin gold film were placed downstream from the ZnO source powder. When the quartz boat was heated at 900°C, composite ZnO-SnO_2 nanostructures were synthesized on the substrate. Figures 1a–1c show scanning electron microscopy (SEM) images of the ZnO-SnO_2 composite structures with different magnifications. Pyramidal SnO_2 nanoparticles with consistent orientation grew on the surface of ZnO nanobelts and aligned along a preferential direction to form a line at the center of the nanobelts. In this study, the nanoparticles are ~100–200 nm in diameter and form an array in the nanobelts with a width ranging from several hundreds of nanometers to several micrometers. Energy-dispersive x-ray (EDX) spectroscopy (Figure 1d) demonstrated the existence of the elements Sn, Zn, and O in the nanoparticles. The Zn comes from the nanobelt matrix. A high-resolution transmission electron microscopy (HRTEM) image of the composite nanobelts (Figure 1e) further demonstrated that the SnO_2 particles grew epitaxially on the $(2\bar{1}\bar{1}0)$ plane of the single-crystal ZnO nanobelts. The growth direction of ZnO nanobelts is determined to be $[01\bar{1}0]$ by the selected-area electron diffraction (SAED) pattern shown in the inset of Figure 1e. From the images, we can see that the (101) planes of SnO_2 nanoparticles are perpendicular to the (0001) planes of ZnO nanobelts and thus parallel to the $(01\bar{1}0)$ planes of ZnO nanobelts. The crystallography relationships thus determined that SnO_2 nanoparticles grew on ZnO nanobelts with the same orientation. The crystallographic relationships are also energetically favorable for the epitaxial growth of SnO_2 nanoparticles on the ZnO nanobelts. The alignment of the SnO_2 particles along the growth direction of the ZnO nanobelts may be due to the existence of planar defects in the nanobelts. In addition, we observed experimentally that SnO_2 nanoparticles can grow at the edge of ZnO nanobelts (Figure 1f). When the reaction temperature increases to 1100°C, composite nanobelts with a random distribution of SnO_2 nanoparticles can be obtained (Figure 1g). From an energy perspective, the planar defects and the edges of ZnO nanobelts have the higher energy, which is the active area for the nucleation of SnO_2. Increasing temperature activates the surfaces of nanobelts, which results in the growth of many randomly oriented SnO_2 particles.

The composite ZnO-SnO_2 nanobelts were used to fabricate a CO gas sensor. As shown in Figure 1h, the composite nanobelts showed reversible and sensitive response to 300 ppm CO at 350°C. The good performance of the gas sensor indicates that composite nanobelts may be a promising gas-sensing material.

Growth of Periodic Zn_2SnO_4 Nanowires

Similarly, we have successfully synthesized periodic single-crystal Zn_2SnO_4 (ZTO) nanowires and twinned nanowires by the VPT process.[14,15] The nanowires were synthesized by thermal evaporation of the mixture of Zn and SnO powder at 1000°C. Figures 2a–2c show SEM images of the ZTO nanowires. The nanowires have diameters mainly ranging from 50 nm to 100 nm and show unique morphologies: rows of inlaid uniform rhombohedral nanocrystals with a consistent orientation, forming uniform steps on their surfaces. The depths of the steps varied in different nanowires, due to variable growth speeds, and ranged from 10 nm to 80 nm. TEM and HRTEM characterizations (Figure 2d) indicate that all the ZTO nanowires are single-crystal and grow along the $[1\bar{1}1]$ direction. Based on the HRTEM results, the surfaces of rhombohedral nanocrystals are determined to be (002), $(\bar{1}11)$ and $(11\bar{1})$. We believe that formation of the single-crystal ZTO nanowires most likely is due to the simultaneous growth along various directions: the rhombohedral nanocrystals grow rapidly along the $[1\bar{1}1]$ direction and extend into nanowires. At the same time, the nanocrystals grow along the directions $[1\bar{1}1]$, $[11\bar{1}]$, and [002], and thus form the periodic nanostructures.

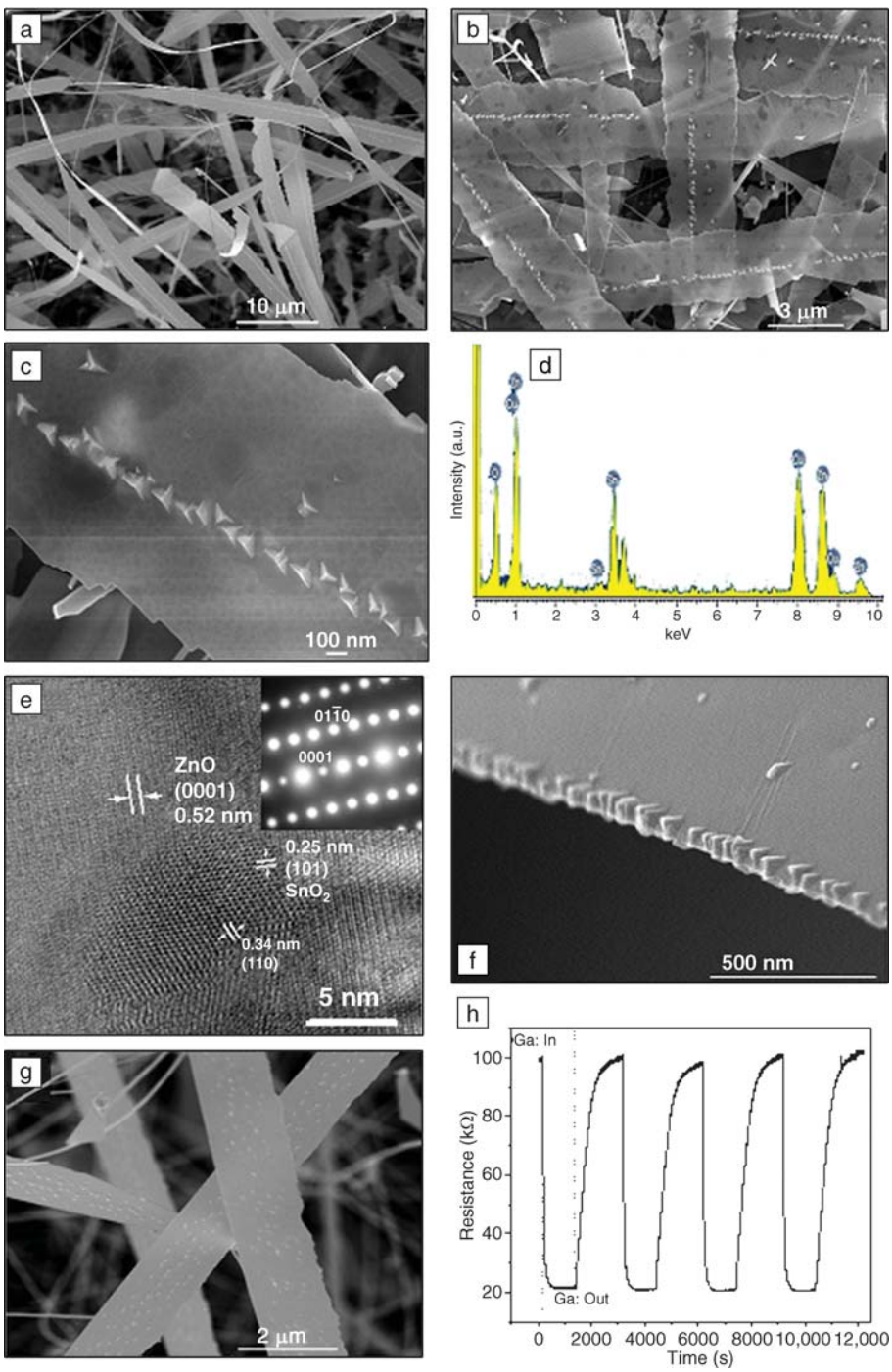

Figure 1. (a)–(c) Scanning electron microscopy (SEM) images of ZnO-SnO_2 nanobelts at different magnifications. (d) Energy-dispersive x-ray spectroscopy of SnO_2 nanoparticles. (e) High-resolution transmission electron micrograph of SnO_2 nanoparticles grown on ZnO belts. Inset shows the diffraction pattern of ZnO nanobelts. (f) SEM image of SnO_2 nanoparticles grown on the edge of ZnO nanobelts. (g) SEM image of disordered SnO_2 nanoparticles grown on ZnO nanobelts. (h) Response of a ZnO-SnO_2 nanobelt gas sensor to 300 ppm CO at 350°C.

It was worth noting that the yield of the single-crystal ZTO nanowires was strongly dependent on the weight ratio of Zn and SnO in the reactants. The yield of ZTO nanowires decreased when the content of Zn in the reactants was reduced. On the other hand, when the ratio of Zn/SnO decreases, periodic twinned nanowires with a zigzag structure can be obtained. The SEM images of the twinned nanowires are shown in Figures 2e–2g.[14] The twinned nanowires were formed by the connection of many uniform octahedral nanocrystals and showed subtle patterns on the surface of the nanowires. TEM and HRTEM characterization suggested that there was a (111) twin between two adjacent octahedral nanocrystals. The (111) twinned crystals have a relative rotational angle, so the periodic appearance of the (111) twins along the nanowire axis yields a zigzag structure (Figure 2h). Figure 2i shows the photoluminescence spectra of the single-crystal and twinned ZTO nanowires. Blue-green emission centered at 490 nm can be observed. However, the UV peaks related to band-to-band transition were not observed.

When the amount of the mixture of Zn and SnO powder was doubled, and a clean silicon wafer without any metal coating was used as the substrate (while other experimental parameters were kept the same), single-crystalline ZTO nanobelts with smooth surfaces were obtained.[16] Shown in Figures 2j and 2k are SEM images of the nanobelts. These nanobelts are several tens of microns in length and several hundred nanometers in width. TEM measurement indicated that

the nanobelts grew along the $[\bar{1}3\bar{3}]$ or $[1\bar{1}1]$ direction. Some of them show ring-like morphologies with typical diameters of 1–5 μm. The nanorings form by the self-coiling and welding of the nanobelts. The growth mechanism of the nanorings may follow that proposed by Wang et al.[17] Based on the SEM and TEM results, it can be seen that various structures were synthesized in a binary oxide system and were strongly dependent on the amount of different precursors in the reactants.

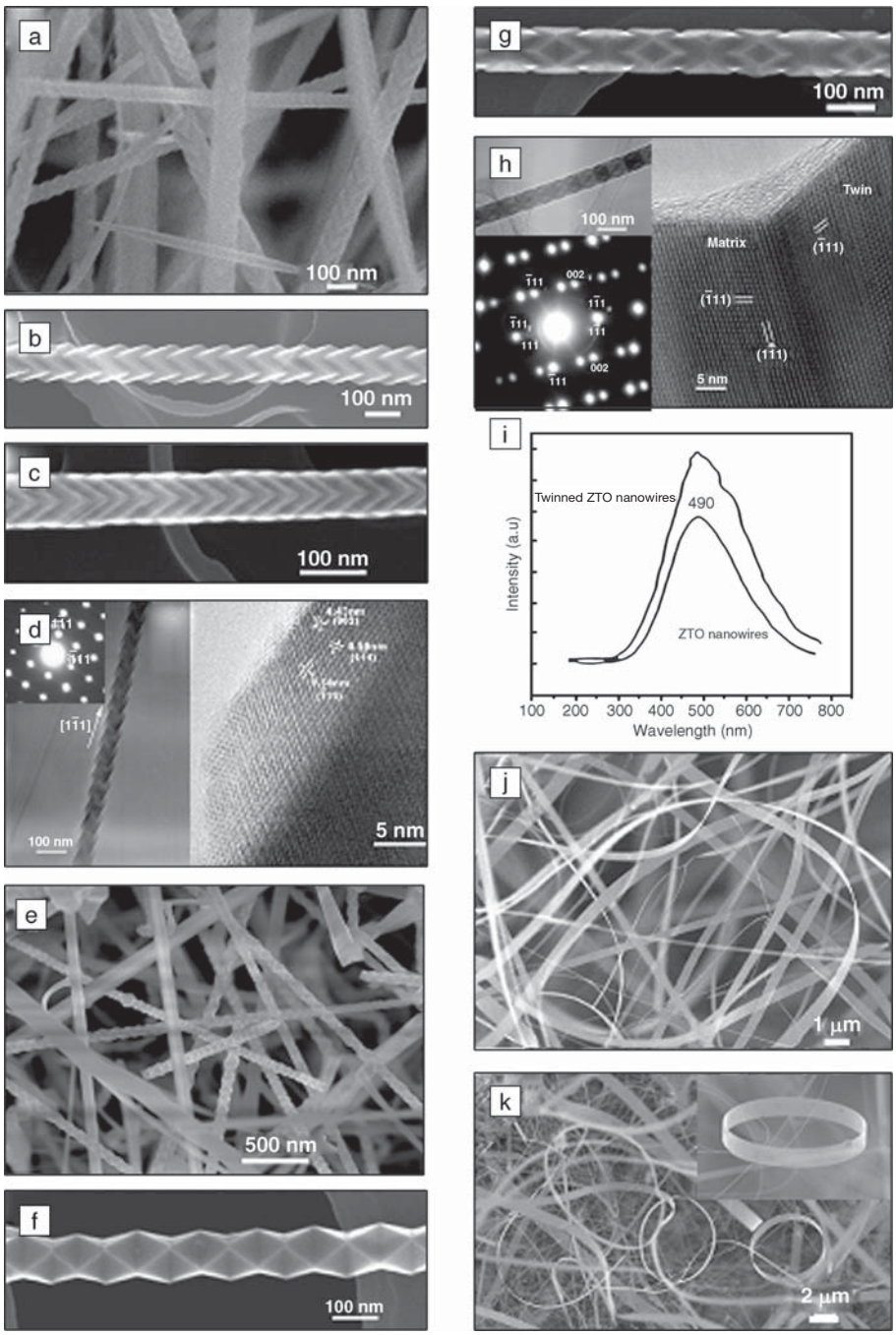

Figure 2. (a)–(c) Scanning electron microscopy (SEM) images of single-crystal ZTO nanowires at different magnifications. (d) Transmission electron microscopy (TEM) image and corresponding selected-area electron diffraction (SAED) pattern of single-crystal ZTO nanowires. (e)–(g) SEM images of twinned ZTO nanowires at different magnifications. (h) TEM and high-resolution TEM images of single-crystal ZTO and the corresponding SAED pattern. (i) Photoluminescence spectrum of twinned ZTO nanowires and single-crystal nanowires excited using a 325-nm He-Gd laser. (j), (k) SEM images of smooth ZTO nanobelts with ring-like structures.

Growth of In_2O_3/SnO_2 Heterojunction Beaded Nanowires

Composite In_2O_3/SnO_2 beaded nanowires can be synthesized by thermal evaporation of SnO and carbon thermal reduction of In_2O_3.[18] In_2O_3/C powders with a weight ratio of 2:1 and SnO powder were put on two parallel quartz boats, respectively, in a horizontal furnace. The reaction was then carried out at two successive temperature stages of 600°C and 900°C. Figures 3a and 3b show SEM images of composite In_2O_3/SnO_2 nanowires with low and high magnifications, respectively. Faceted beads grown on core nanowires along a consistent orientation were observed. The core nanowires have a diameter of about 100–200 nm, while the In_2O_3 nanoparticles have a diameter of 200–300 nm. The corresponding SAED pattern of the beaded nanowires is shown in Figure 3c. Two sets of diffraction spots are observed in the diffraction pattern. One is indexed to be rutile SnO_2 and the other is indexed to be cubic In_2O_3. The SAED result suggests that the nanowires consist of two different materials. Figure 3d shows an HRTEM image of the interface between the bead and the core nanowire. A clear and smooth interface between SnO_2 nanowires (left side) and In_2O_3 nanoparticles (right side) can be observed. From the HRTEM image and SAED pattern, the orientation relationships between the two crystals can be determined as follows: $[0\bar{1}1]_{In_2O_3} \| [010]_{SnO_2}$, $(\bar{1}01)_{SnO_2} \| (222)_{In_2O_3}$, and $(200)_{SnO_2} \| (200)_{In_2O_3}$. At these definite orientations, the lattice mismatch dislocation between two crystals will be small. In addition, the lattice dimensions of these facets are almost identical to each other. The good lattice match thus facilitates the formation of heterojunctions of In_2O_3 and SnO_2.

The schematic shown in Figure 3e depicts the formation process of composite nanowires. The SnO_2 nanowires first form at the first temperature stage, followed by the In_2O_3 particles attached on the surface of SnO_2 nanowires. These In_2O_3 particles eventually developed into the faceted crystals. This two-stage VPT method has advantages for the synthesis of binary oxide nanowires. At each temperature stage, one reaction dominates. Changing the vapor precursor can be expected to lead to synthesis of various binary oxide structures.

Figure 3f shows the room-temperature photoluminescence (PL) spectra of the beaded nanowires, indicating the wide

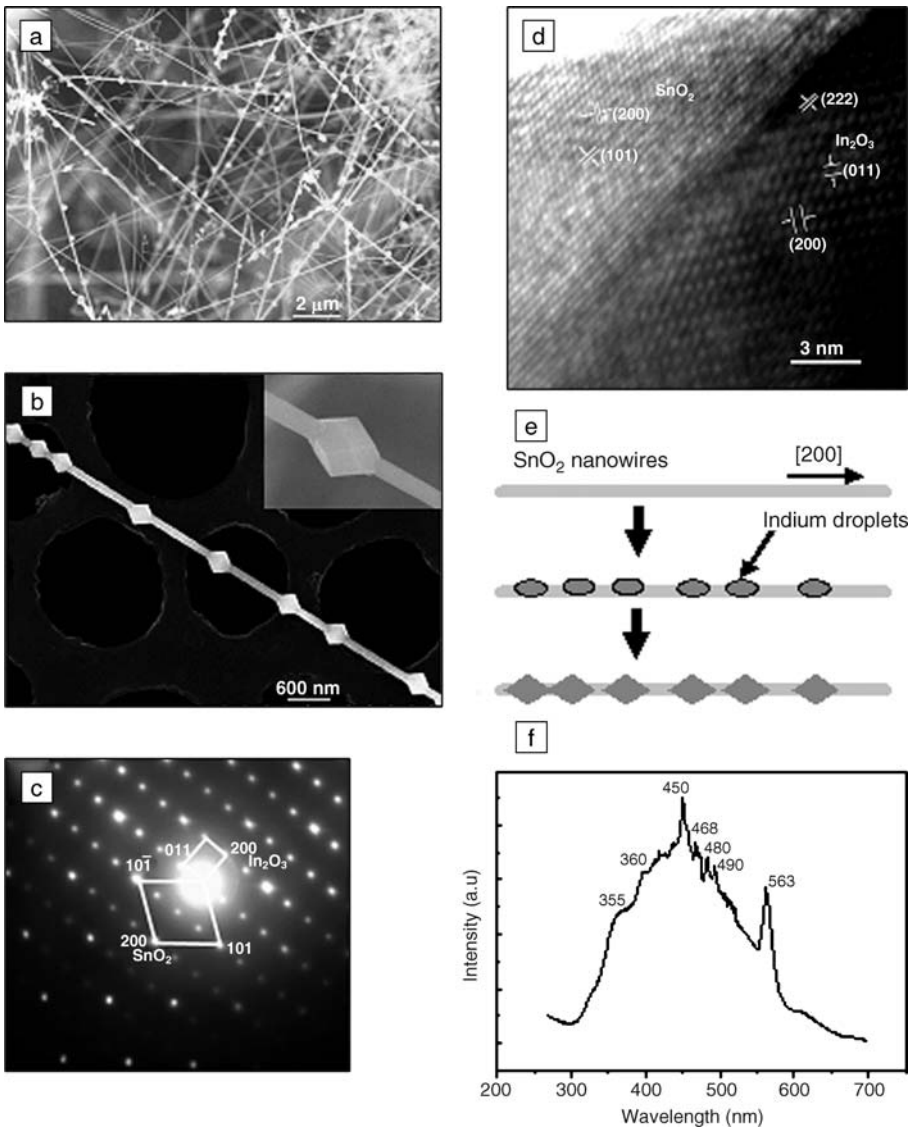

Figure 3. (a), (b) Scanning electron microscopy (SEM) images of SnO_2-In_2O_3 composite nanowires at low and high magnification, respectively. (c) Selected-area electron diffraction (SAED) pattern of a composite nanowire, showing two sets of spots indexed to be In_2O_3 and SnO_2, respectively. (d) High-resolution transmission electron micrograph of the interface between In_2O_3 bead and SnO_2 core nanowires. (e) Schematic illustration of the formation process of composite nanowires. (f) Photoluminescence spectrum of SnO_2-In_2O_3 composite nanowires.

range of photoluminescence peaks ranging from ultraviolet to green emission that can be observed. Most of the peaks are ascribed to the emission of SnO_2 and In_2O_3.[17] In addition, a new peak at 450 nm is observed that has not been reported in the literature; the origin of this peak is currently not clear. These emissions are not caused by the band-to-band transition, which can be attributed to other luminescence centers, such as oxygen vacancies, defects in the interface, and doping impurities in the composite beaded nanowires.

Conclusion

In summary, we described a simple VPT method for controlled synthesis of one-dimensional binary oxide nanostructures including ZnO/SnO_2, ZTO, and SnO_2/In_2O_3 composite nanostructures. We analyzed some of the key issues facing the practical realization of binary oxide nanowires from a synthesis point of view. Using the modified VPT method and controlling the reaction parameters, some binary oxide nanostructures with designed compositions and various morphologies can be obtained. Although the shape and size control of the 1D binary oxide nanowires is far from satisfactory, this simple synthesis method paves the way for the investigation of growth behavior of binary oxide nanostructures and provides promising materials for building functional nanodevices.

Acknowledgments

The authors would like to thank the National Natural Science Foundation of China (Grant No. 10334060 and 50572119) and the "973" National Key Basic Research Program of China (Grant No. 2005CB623602) for financial support.

References

1. M.H. Huang, S. Mao, H. Feick, H.Q. Yan, Y.Y. Wu, H. Kind, E. Weber, R. Russo, and P.D. Yang, *Science* **292** (2001) p. 1897.
2. A. Kolmakov, Y.X. Zhang, G.S. Cheng, and M. Moskovits, *Adv. Mater.* **15** (2003) p. 997.
3. C. Li, D.H. Zhang, S. Han, X.L. Liu, T. Tang, and C.W. Zhou, *Adv. Mater.* **15** (2003) p. 143.
4. Y.N. Xia, P.D. Yang, Y.G. Sun, Y.Y. Wu, B. Mayers, B. Gates, Y.D. Yin, F. Kim, and Y.Q. Yan, *Adv. Mater.* **15** (2003) p. 353.
5. Y.Y. Wu, R. Fan, and P.D. Yang, *Nano Lett.* **2** (2002) p. 83.
6. J.Y. Lao, J.G. Wen, and Z.F. Ren, *Nano Lett.* **2** (2002) p. 1287.
7. M.S. Gudiksen, L.J. Lauhon, J.F. Wang, D.C. Smith, and C.M. Lieber, *Nature* **415** (2002) p. 617.
8. J.X. Wang, D.F. Liu, X.Q. Yan, H.J. Yuan, L.J. Ci, Z.P. Zhou, Y. Gao, L. Song, L.F. Liu, W.Y. Zhou, G. Wang, and S.S. Xie, *Solid State Commun.* **130** (2004) p. 89.
9. D.F. Liu, Y.J. Xiang, Z.X. Zhang, J.X. Wang, Y. Gao, L. Song, L.F. Liu, X.Y. Dou, X.W. Zhao, S.D. Luo, C.Y. Wang, W.Y. Zhou, G. Wang, and S.S. Xie, *Nanotechnology* **16** (2005) p. 2665.
10. P.X. Gao, Y. Ding, W. Mai, W.L. Hughes, C.S. Lao, and Z.L. Wang, *Science* **309** (2005) p. 1700.
11. Z.R. Dai, J.L. Gole, J.D. Stout, and Z.L. Wang, *J. Phys. Chem. B* **106** (2002) p. 1274.
12. Z.W. Pan, Z.R. Dai, and Z.L. Wang, *Science* **291** (2001) p. 1947.
13. J.X. Wang, PhD thesis, Institute of Physics, Chinese Sciences Academy, Beijing (2005).
14. J.X. Wang, S.S. Xie, Y. Gao, X.Q. Yan, D.F. Liu, H.J. Yuan, Z.P. Zhou, L. Song, L.F. Liu, W.Y. Zhou, and G. Wang, *J. Cryst. Growth* **267** (2004) p. 177.
15. H.Y. Chen, J.X. Wang, H.C. Yu, H.X. Yang, S.S. Xie, and J.Q. Li, *J. Phys. Chem. B* **109** (2005) p. 2573.
16. J.X. Wang, S.S. Xie, H.J. Yuan, X.Q. Yan, D.F. Liu, Y. Gao, Z.P. Zhou, L. Song, L.F. Liu, X.W. Zhao, X.Y. Dou, W.Y. Zhou, and G. Wang, *Solid State Commun.* **131** (2004) p. 435.
17. X.Y. Kong, Y. Ding, R.S. Yang, and Z.L. Wang, *Science* **303** (2004) p. 1348.
18. J.X. Wang, H.Y. Chen, Y. Gao, D.F. Liu, L. Song, Z.X. Zhang, X.W. Zhao, X.Y. Dou, S.D. Luo, W.Y. Zhou, G. Wang, J.Q. Li, and S.S. Xie, *J. Cryst. Growth* **284** (2005) p. 73. □